Inorganic Chemistry

Article

pubs.acs.org/IC

O_2 Insertion into Group 9 Metal–Hydride Bonds: Evidence for Oxygen Activation through the Hydrogen-Atom-Abstraction Mechanism

Jason M. Keith,*[,†] Thomas S. Teets,[‡] and Daniel G. Nocera[‡]

[†]Theoretical Division, MS B268, Los Alamos National Laboratory, Los Alamos, New Mexico 87545, United States

[‡]Department of Chemistry, 6-335, Massachusetts Institute of Technology, 77 Massachusetts Avenue, Cambridge, Massachusetts 02139-4307, United States

Supporting Information

ABSTRACT: A detailed density functional study was performed to examine the reaction of mixed-valence dirhodium and diiridium species $[M_2^{0,II}(tfepma)_2(CN^tBu)_2(Cl)_2$ (**1**, tfepma = MeN[P-$(OCH_2CF_3)_2]_2$, CN^tBu = *tert*-butyl isocyaninde)] with HCl and oxygen with an interest in examining the pathways for oxygen insertion into the intermediate metal hydride to form hydroperoxo species. The O_2 hydrogen atom abstraction mechanism for both the Rh and Ir was found to be feasible. This is the first time this mechanism has been applied to a Rh system and only the second time it has been examined for a system other than Pd. The competing *trans* HCl reductive elimination pathway was also examined and found to be greatly dependent on the stereochemistry of the starting hydride primarily due to the intermediate formed upon the loss of Cl^-. As a result, the reductive elimination pathway was more favorable by 11.5 kcal/mol for the experimentally observed Ir stereoisomer, while the two pathways were isoenergetic for the other stereoisomer of the Rh complex. All findings are consistent with the kinetics study previously performed.

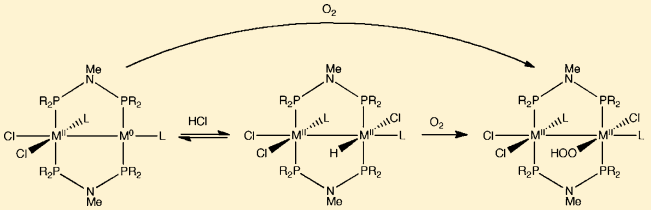

INTRODUCTION

A fuel cell recovers stored energy in the form of hydrogen via a four-proton, four-electron reduction of oxygen at the cathode.[1] In an effort to understand this mechanistically complex chemistry, much work has been performed over the last quarter century to develop molecular analogues for the study of oxygen reduction.[2] In biology, oxidase enzymes such as cytochrome c oxidase perform this same chemistry using oxygen as the terminal oxidant.[3] By employing oxygen in this same way, a rich array of aerobic oxidation chemistry has been developed employing palladium catalysts.[4] In all of these chemistries, understanding the precise nature of the reaction of O_2 with the given metal complex is crucial to further understanding and advancing these systems.

Mononuclear hydroperoxo intermediates play a significant role in homogeneous oxidation chemistry utilizing oxygen.[5] There have been several mechanistic pathways proposed for the formation of these key intermediates (Scheme 1), and a substantial amount of recent research has been directed at understanding these processes and elucidating the factors that govern these reactions.[6−15] A well-established mechanism for O_2 insertion into metal hydride bonds is the Reductive Elimination (**RE**) pathway outlined in Scheme 1. This mechanism proceeds through the reductive elimination of HX from the M^n complex to form a reduced M^{n-2} complex, which then adds oxygen before the reincorporation of HX to form the corresponding metal–hydroperoxo. Stahl and co-workers have been a major contributor to the examination of the **RE** pathway with Pd–H complexes[6] and the interaction of oxygen with Pd^0.[7] An important feature of these HX **RE** processes is that the formal two-electron reduction of the metal accompanies a formal two-electron oxidation of the "hydride" to a proton. Thus, the overall process is consistent with the deprotonation of the M–H species by ligand X^-. This distinction is important as it demonstrates the obvious parallels of **RE** with the Base Catalyzed O_2 insertion process (Scheme 1, **BC**), as recently discussed by Szajna-Fuller and Bakac.[8] In this mechanism, M–H is deprotonated by an exogenous base, Y, followed by the addition of O_2 to form the superoxo, which is then protonated by HY^+ to furnish the metal–hydroperoxo and Y. While in Scheme 1, X^- is shown staying ligated to M, this is not necessary. In the case of loss of X^-, the reaction would proceed similarly to the **RE** pathway with oxidation by oxygen followed by protonation and reintroduction of X^-. The crossover between these mechanisms has been examined in detail for Pd(X)H (X = OAc, Cl) where OAc^- acts as ancillary ligand and base while Cl^- requires an exogenous base.[9]

While these two mechanisms result from a loss of H^+, another established mechanistic route is the Radical Chain mechanism (Scheme 1, **RC**). This process requires a radical initiator $Z^\bullet$ (or light) to abstract an H atom to produce the

Received: June 19, 2012
Published: August 10, 2012

   dx.doi.org/10.1021/ic301303n | *Inorg. Chem.* 2012, 51, 9499–9507

Scheme 1

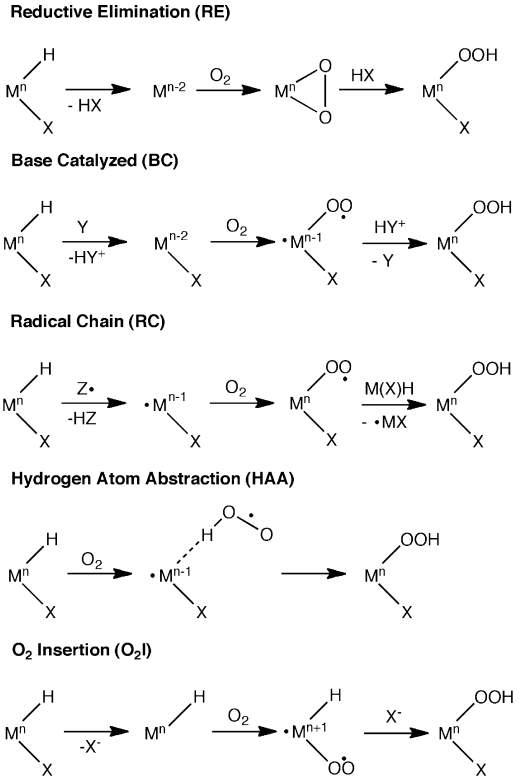

one-electron reduced M• complex. This complex then reacts with O_2 to form a superoxo, which then abstracts a hydrogen atom in a radical propagation step to form the metal–hydroperoxo. In Scheme 1, the H atom donor employed in the propagation step is represented by a second M–H species. Bakac has studied this process extensively for Rh–H,[10] while Goldberg and co-workers have observed a similar process at work for Pt–H.[11]

A parallel radical rebound process can be envisioned in which radical initiation by Z• to form HZ is followed immediately by rebound to form a •M–ZH complex. Can triplet oxygen act as the radical initiator? In 2005, one of us (J.M.K.) first proposed a controversial mechanism in which triplet oxygen was the radical initiator. Molecular oxygen insertion into a Pd–H bond occurs by first abstracting a hydrogen atom from the metal center and then rebounding to form the palladium hydroperoxo (Scheme 1, **HAA**).[9a] This reaction was initially termed direct insertion with a focus on the overall results of the process but has become known as Hydrogen Atom Abstraction (**HAA**) in an effort to reflect the steps involved. While this mechanism has recently been shown not to be active in the original system it was proposed for,[12] it has since become generally accepted as the active mechanism for the Pd–H pincer system studied by Kemp and co-workers.[9b,13] Much work has been done examining various aspects of this **HAA** mechanism for Pd–H complexes by one of us (J.M.K.)[9] and most notably by the groups of Stahl[14] and Russo.[15] Recently, Sha et al. presented a heterogeneous analog to this process by which oxygen activation occurs when O_2 adsorbed on a Pd surface abstracts a hydrogen atom from a surface hydride prior to O–O dissociation, further demonstrating the versatility of the **HAA** process.[16] Whereas the examination of the **HAA** mechanism has primarily focused on Pd, in 2006 Cui and Wayland published a kinetic examination of the reaction of a (porphyrin)Rh–H that demonstrates the kinetics for a "near concerted" insertion of O_2 to the Rh–H, which could conceivably occur by **HAA**.[17] Insertion of O_2 into an Ir–H bond has been proposed by Arita et al.,[18] and Chowdhury et al. have recently examined the **HAA** process for a similar Ir–H system.[19]

One final possibility arises from keeping the M–H bond intact and forming a superoxo complex through the addition of oxygen to a coordinatively unsaturated metal hydride accompanied by a subsequent hydrogen migration/O_2 insertion step (Scheme 1, $\mathbf{O_2I}$). Whereas Scheme 1 illustrates this through an initial loss of the ancillary ligand X^-, this is not necessary for coordinatively unsaturated hydride complexes, such as the addition of oxygen to a square planar metal hydride to form a five-coordinate superoxo complex.

Recently, Teets et al. reported mixed-valent dirhodium complex $\mathbf{1_{Rh}}$, which upon treatment with HCl established an equilibrium between two isomeric hydride species ($\mathbf{2_{Rh}}$ and $\mathbf{3_{Rh}}$, Scheme 2).[20] $\mathbf{2_{Rh}}$ and $\mathbf{3_{Rh}}$ were found to be stable in the presence of excess HCl, and the introduction of O_2 resulted in conversion to $\mathbf{4_{Rh}}$ and water.

Scheme 2

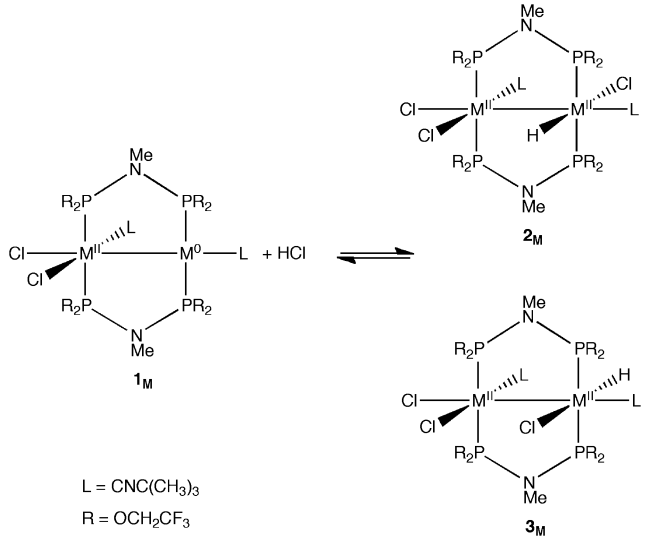

In subsequent work, Teets et al. made the analogous di-iridium complexes and performed a detailed mechanistic study examining the reaction of the Rh and Ir hydride species with O_2 and HCl.[21] Interestingly, in the Ir system only one hydride species was observed, $\mathbf{3_{Ir}}$. The reaction of $\mathbf{2_{Rh}}/\mathbf{3_{Rh}}$ with O_2 and HCl to form $\mathbf{4_{Rh}}$ (Scheme 3) exhibited a complex three-term rate law, eq 1. Radical initiators were found to have no effect on the kinetics, thus eliminating the **RC** process while the acidic conditions present eliminate the **BC** process. The first term

Scheme 3

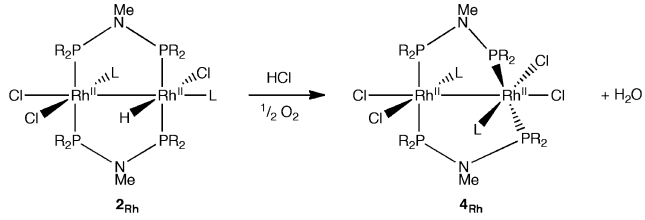

dx.doi.org/10.1021/ic301303n | Inorg. Chem. 2012, 51, 9499–9507

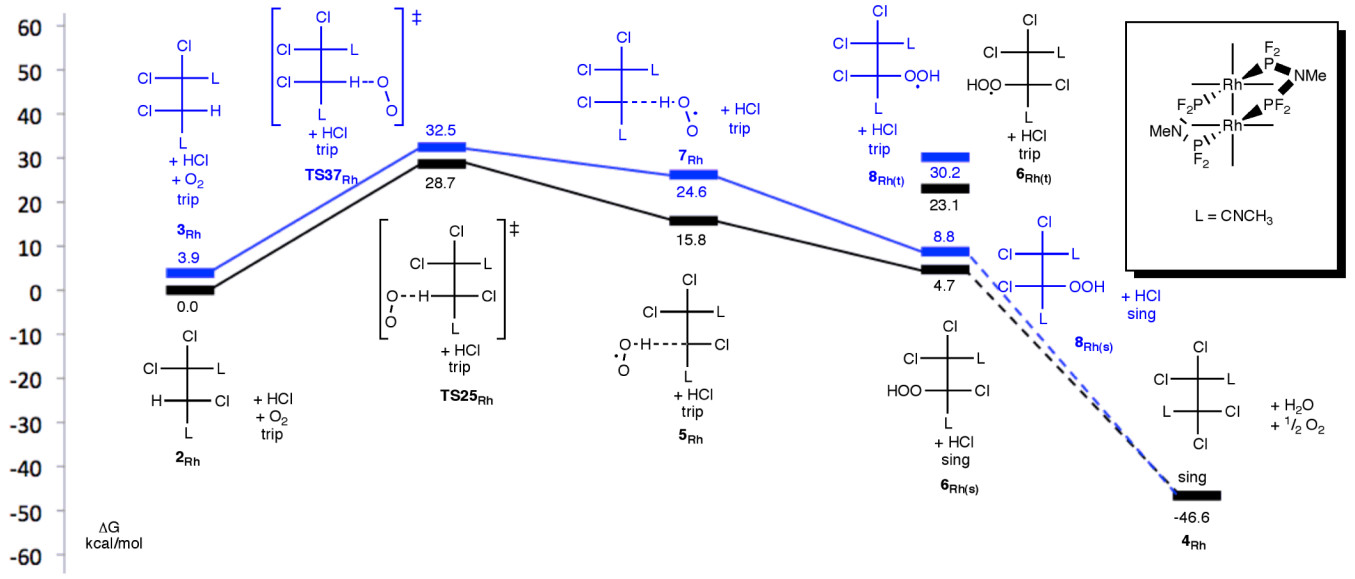

Figure 1. Calculated potential energy surface for Rh−H complex + O_2 hydrogen atom abstraction pathway for species $\mathbf{2}_{Rh}$ and $\mathbf{3}_{Rh}$. The observed isomer $\mathbf{2}_{Rh}$ set to 0.0.

indicates a reaction that is first-order in O_2 and complex and inverse first order in HCl, consistent with a **RE** pathway that involves a pre-equilibrium reductive elimination of HCl followed by the rate-limiting addition of O_2. The second term is simply first order with respect to the complex and O_2, suggesting the insertion of O_2 into the Rh−H bond possibly through a **HAA** process. The third term is first order in complex only and represents a third mechanistic pathway that could arise from rate-limiting reductive elimination of HCl.

$$\text{Rate} = k_1\frac{[\mathbf{2}_{Rh}][O_2]}{[HCl]} + k_1'[\mathbf{2}_{Rh}][O_2] + k_1''[\mathbf{2}_{Rh}] \quad (1)$$

$$\text{Rate} = k_2\frac{[\mathbf{3}_{Ir}][O_2]}{[HCl]} \quad (2)$$

In contrast to these results, the reaction of $\mathbf{3}_{Ir}$ with O_2, which forms an isolable hydroperoxo complex, exhibited a one-term rate law, eq 2. The rate law indicates a reaction that is first-order in O_2 and complex and inverse first order in HCl similar to the first term in eq 1. Again, this is consistent with a **RE** pathway consisting of reductive elimination of HCl followed by the rate-limiting addition of O_2.

These kinetic studies pose several important questions. What is the origin of the differences between the rate laws for the Rh and Ir complexes? What is the mechanism at play that gives rise to the second term in the Rh rate law, which suggests the insertion of O_2 directly into the Rh−H bond? Could this possibly be through a **HAA** process, which has seldom been invoked for systems other than Pd hydrides and never for Rh? Herein, we examine these questions using modern density functional theory. We examine in detail the feasibility of a **HAA** process for the insertion of O_2 into these Rh−H and Ir−H bonds and compare this process directly with the formation of $\mathbf{1}_M$ along a **RE** pathway.

RESULTS AND DISCUSSION

Hydrogen Atom Abstraction Pathway. We performed an examination of the **HAA** mechanistic pathway beginning at the $Rh_2^{II,II}$ species $\mathbf{2}_{Rh}$ (black path, Figure 1). A transition state corresponding to a hydrogen-atom abstraction by oxygen was located, $\mathbf{TS25}_{Rh}$, with $\Delta G^{\ddagger}$ = 28.7 kcal/mol. In this transition state, the Rh−H bond has stretched to 1.78 Å from 1.55 Å in $\mathbf{2}_{Rh}$, and the new O−H distance is 1.24 Å. In addition, the O−O distance has increased from a calculated value of 1.20 Å in O_2 to 1.25 Å. Spin densities show a total of 1.6 unpaired electrons on the O_2 fragment demonstrating that this is a H-atom abstraction (i.e., the proton transfer is coupled with an electron transfer along a synchronous reaction coordinate).

From $\mathbf{TS25}_{Rh}$, an intermediate is found that consists of a van der Waals complex of $Rh_2^{II,I}$ species and HO_2, $\mathbf{5}_{Rh}$. Spin densities now show 0.6 unpaired electrons on the Rh^{I} center (0.0 on Rh^{II}) and 1.2 electrons on the HO_2 moiety with the remaining spin density residing on the Cl formerly *trans* to the hydride. From here, a spin crossing to the singlet surface (see below) along with a rotation of HO_2 results in the singlet $Rh_2^{II,II}$ hydroperoxo species, $\mathbf{6}_{Rh(s)}$, with ΔG = 4.7 kcal/mol (ΔG = 23.1 kcal/mol for the corresponding triplet $\mathbf{6}_{Rh(t)}$).

From $\mathbf{6}_{Rh(s)}$, the reaction is calculated to be thermodynamically downhill 51.3 kcal/mol to form the $Rh_2^{II,II}Cl_4$ complex, $\mathbf{4}_{Rh}$, one equivalent of water, and half an equivalent of oxygen. As we are focused here on the steps resulting in the insertion of oxygen to form the hydroperoxo species, we have not examined the conversion of the hydroperoxo to products, but the large exothermicity of these remaining steps suggests that they do not affect the overall kinetics, consistent with the observed rate laws.

In a similar fashion, the mechanistic pathway from species $\mathbf{3}_{Rh}$ was optimized and is also presented in Figure 1 (blue path). Species $\mathbf{3}_{Rh}$ was found to be 3.9 kcal/mol higher in energy than species $\mathbf{2}_{Rh}$, and that difference was found to track almost exactly through the accompanying transition state ($\Delta\Delta G^{\ddagger}$ = 3.8 kcal/mol). As these reaction profiles are almost identical, this second pathway will not be discussed further.

These results strongly suggest that the **HAA** process is feasible for both of these Rh−H complexes, suggesting that the second term in eq 1 is in fact due to **HAA**. In order to understand why the analogous term is not present in eq 2, the parallel **HAA** pathways were calculated for the $Ir_2^{II,II}$ species $\mathbf{2}_{Ir}$ and $\mathbf{3}_{Ir}$ (black and blue paths, Figure 2). While in the Rh system

dx.doi.org/10.1021/ic301303n | Inorg. Chem. 2012, 51, 9499−9507

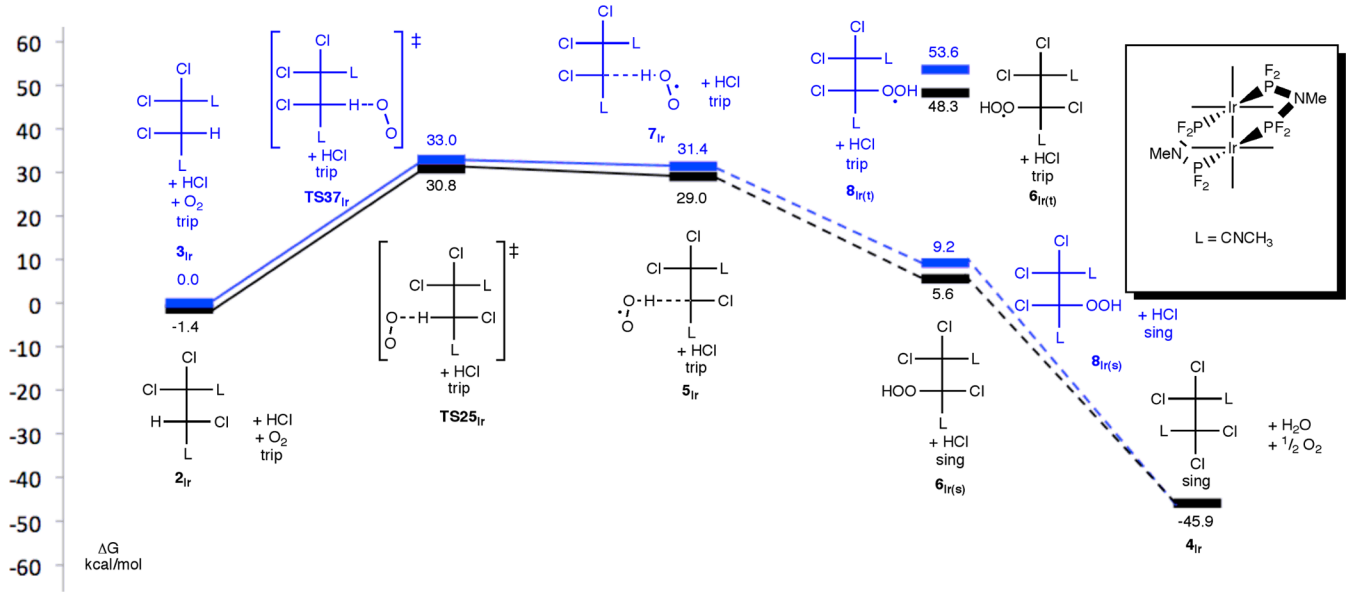

Figure 2. Calculated potential energy surface for Ir−H complex + O_2 hydrogen atom abstraction pathway for species $\mathbf{2}_{Ir}$ and $\mathbf{3}_{Ir}$. The observed isomer $\mathbf{3}_{Ir}$ set to 0.0.

Teets et al. examined the reaction of $\mathbf{2}_{Rh}$, the other isomer, $\mathbf{3}_{Ir}$, was isolated in the Ir system. To keep track of this fact, species $\mathbf{3}_{Ir}$ has been set to 0.0 kcal/mol in Figure 2.

Not surprisingly, the calculated **HAA** mechanism for the Ir system is similar to that of the Rh. The major difference is a $\Delta G^{\ddagger}$ that is higher by ~4.5 kcal/mol, resulting in values of 32.2 and 33.0 kcal/mol for $\mathbf{2}_{Ir}$ and $\mathbf{3}_{Ir}$. This augmentation in $\Delta G^{\ddagger}$ is consistent with the expected increase in M−H bond strength for the iridium hydride complex compared to its rhodium hydride congener.[22] While an increase in $\Delta G^{\ddagger}$ by 4.5 kcal/mol would substantially slow down the **HAA** process for these Ir complexes, it should not completely shut off the **HAA** process for the Ir system altogether.

Spin Crossover. In an attempt to gain further insight into the triplet/singlet spin-crossing event in the **HAA** process, the singlet and triplet surfaces were examined in further detail in the vicinity of $\mathbf{5}_M/\mathbf{6}_M$ and $\mathbf{7}_M/\mathbf{8}_M$ (Figure 3, Table 1). From the optimized geometry for $\mathbf{5}_{Rh(t)}$, a single-point energy was obtained for $\mathbf{5}_{Rh(s)}\mathbf{sp}$, and the singlet/triplet gap was found to be only 1.6 kcal/mol at this point, an energy difference that is within the errors in methods. These surfaces can be considered

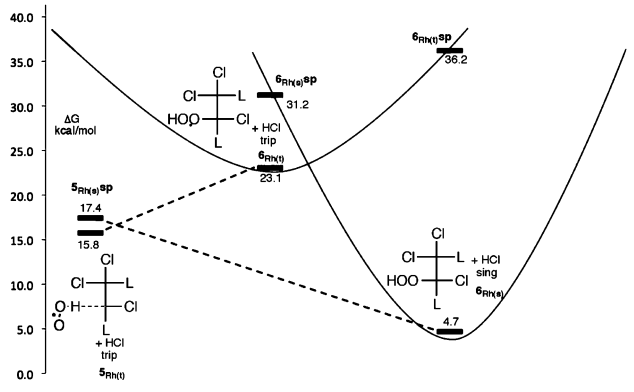

Figure 3. Detailed view of the singlet and triplet surfaces in the vicinity of $\mathbf{5}_{Rh}$ and $\mathbf{6}_{Rh}$. Structures labeled **sp** are single-point calculations performed at the geometry optimized for the other spin state.

Table 1. Energy Values (kcal/mol) for Singlet and Triplet Surfaces in the Vicinity of the Spin Crossing for $\mathbf{5}_M$−$\mathbf{8}_M$

$\mathbf{5}_{Rh(t)}$	$\mathbf{6}_{Rh(t)}$	$\mathbf{6}_{Rh(t)}\mathbf{sp}$
15.8	23.1	36.2
$\mathbf{5}_{Rh(s)}\mathbf{sp}$	$\mathbf{6}_{Rh(s)}\mathbf{sp}$	$\mathbf{6}_{Rh(s)}$
17.4	31.2	4.7
$\mathbf{7}_{Rh(t)}$	$\mathbf{8}_{Rh(t)}$	$\mathbf{8}_{Rh(t)}\mathbf{sp}$
24.6	30.2	43.4
$\mathbf{7}_{Rh(s)}\mathbf{sp}$	$\mathbf{8}_{Rh(s)}\mathbf{sp}$	$\mathbf{8}_{Rh(s)}$
24.8	27.3	8.8
$\mathbf{5}_{Ir(t)}$	$\mathbf{6}_{Ir(t)}$	$\mathbf{6}_{Ir(t)}\mathbf{sp}$
29.0	48.3	62.7
$\mathbf{7}_{Ir(s)}\mathbf{sp}$	$\mathbf{8}_{Ir(t)}$	$\mathbf{8}_{Ir(t)}\mathbf{sp}$
30.6	53.6	68.9
$\mathbf{7}_{Ir(t)}$	$\mathbf{8}_{Ir(s)}\mathbf{sp}$	$\mathbf{8}_{Ir(s)}$
31.4	35.1	9.2
$\mathbf{7}_{Ir(s)}\mathbf{sp}$	$\mathbf{8}_{Ir(t)}$	$\mathbf{8}_{Ir(t)}\mathbf{sp}$
33.2	53.6	68.9

approximately isoenergetic at this point along the reaction coordinate. Fundamentally, this makes sense as the two radicals in species $\mathbf{5}_M$ are localized on different molecular fragments and are expected to have little interaction.

Evaluation of species $\mathbf{5}_{Rh(s)}\mathbf{sp}$ showed a negative frequency corresponding to HO_2 rotating with respect to the $Rh_2^{II,I}$ molecule. Optimizing this species results in the formation of $\mathbf{6}_{Rh(s)}$, identical to what was observed in the original Pd system studied.[9a] Single-point calculations were performed for species $\mathbf{6}_{Rh(s)}$ and $\mathbf{6}_{Rh(t)}$ with the other spin state and are presented in Figure 3 in order to provide a clear picture of these potential energy surfaces in this region. The corresponding values for all six species illustrated in Figure 3 for both Rh and Ir isomers are presented in Table 1. It should be noted that the singlet/triplet gap at $\mathbf{5}_{M(t)}/\mathbf{7}_{M(t)}$ is <2 kcal/mol for all four species. In short, the calculations suggest a facile spin crossover in these systems, such that all elementary steps following $\mathbf{5}_{M(s)}/\mathbf{7}_{M(s)}$ proceed via the singlet surface.

dx.doi.org/10.1021/ic301303n | Inorg. Chem. 2012, 51, 9499−9507

Reductive Elimination Pathway. In order to gain further insight into the absence of a **HAA** pathway in the rate law from the Ir system, we set out to understand the factors governing the reductive elimination of HCl from species $\mathbf{2_M}$ and $\mathbf{3_M}$ to go back to $\mathbf{1_M}$ and the subsequent addition of O_2. Reductive elimination from a *trans* octahedral complex is not straightforward. The two primary pathways resulting in an overall reductive elimination are (1) rearrangement to a *cis* species followed by a concerted reductive elimination step and (2) conversion of one ligand (in this case Cl^-) from inner-sphere to outer-sphere, migration around the molecule, and reductive coupling with the other ligand (in this case simply deprotonation of M−H). In these systems, rearrangement to the *cis* conformation was not observed experimentally. In addition, chloride ligands *trans* to hydrides are known to be highly labile, as previously demonstrated in a similar monometallic *trans*-(cyclam)Rh(H)Cl species studied first by Bakac and co-workers.[23,24] Locating the outer-sphere chloride complex and the deprotonation transition states that correspond to the loss of HCl for these *trans* complexes proved to be exceedingly difficult, and removal of the Cl^- from $\mathbf{2_M}$ and $\mathbf{3_M}$ resulted in two new intermediates $\mathbf{9_M}$ and $\mathbf{10_M}$ (Figures 4 and 5). Examination of the potential energy surfaces

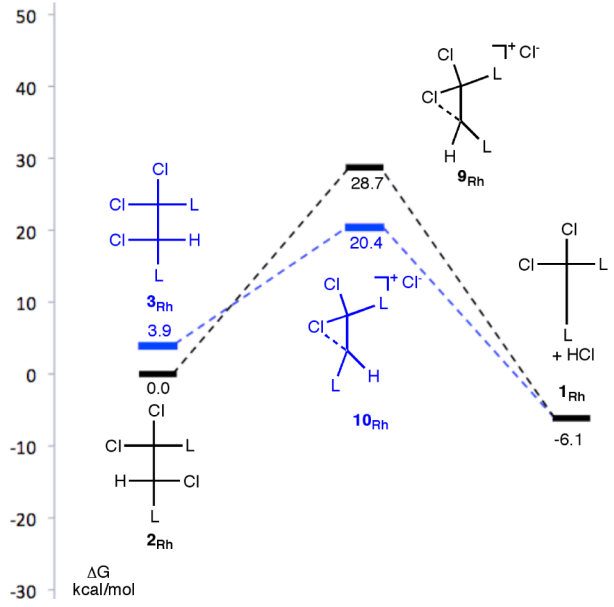

Figure 4. Calculated potential energy surface for Rh−H complex reductive elimination pathway for species $\mathbf{2_{Rh}}$ and $\mathbf{3_{Rh}}$.

around these species revealed either of two results: if the Cl^- was placed opposite the H, the energy was found to decrease monotonically to species $\mathbf{2_{Rh}}/\mathbf{3_{Rh}}$, whereas if the Cl^- was placed near the H, the energy was found to decrease monotonically to species $\mathbf{1_{Rh}}$. While Figure 6 illustrates scans along the gas-phase potential energy surface, these outer-sphere chloride complexes were found to be unstable when examined in solvent as well. This suggested that the conversions of $\mathbf{9_{Rh}}$ and $\mathbf{10_{Rh}}$ back to $\mathbf{2_{Rh}}$ and $\mathbf{3_{Rh}}$ or to $\mathbf{1_{Rh}}$ are barrier-less or near barrier-less steps. We therefore accepted the energies of intermediates $\mathbf{9_{Rh}}$ and $\mathbf{10_{Rh}}$ as approximate barriers for the reductive elimination steps.

From species $\mathbf{1_{Rh}}$, the addition of O_2 to form the triplet $Rh_2^{II,I}$−superoxo, $\mathbf{11_{Rh}}$, was found to be uphill 18.1 kcal/mol (Figure 7). Conversion to the singlet spin state results in the formation of the η^2-peroxo-$Rh_2^{II,II}$ complex (see below), $\mathbf{12_{Rh}}$,

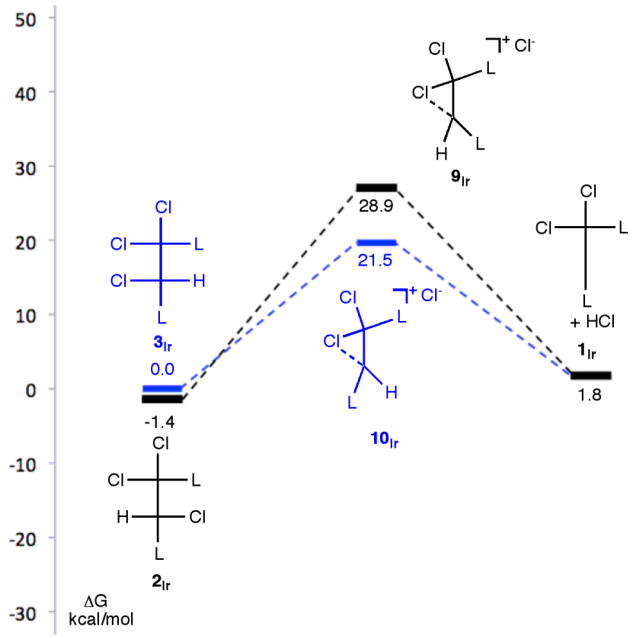

Figure 5. Calculated potential energy surface for Ir−H complex reductive elimination pathway for species $\mathbf{2_{Ir}}$ and $\mathbf{3_{Ir}}$.

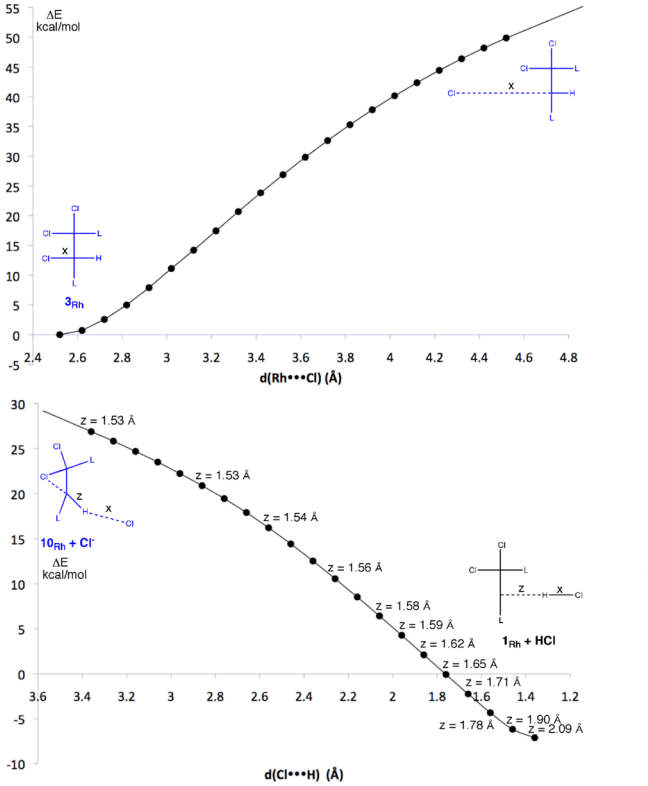

Figure 6. Scan of Rh−Cl distance in $\mathbf{3_{Rh}}$ (top) and scan of H−Cl distance in $\mathbf{1_{Rh}}$·H−Cl complex (bottom, Rh−H distances labeled as *z*).

which is 23.0 kcal/mol uphill from $\mathbf{1_{Rh}}$. Again a barrier for the addition of HCl was not found as any attempts to protonate the O in the presence of Cl^- resulted in either the release of HCl or the formation of the hydroperoxo, $\mathbf{6_{Rh(s)}}$. A parallel pathway was found leading to the formation of $\mathbf{8_{Rh(s)}}$ through the addition of oxygen to the opposite side of the Rh^0 center (Figure 7, blue path).

dx.doi.org/10.1021/ic301303n | *Inorg. Chem.* 2012, 51, 9499−9507

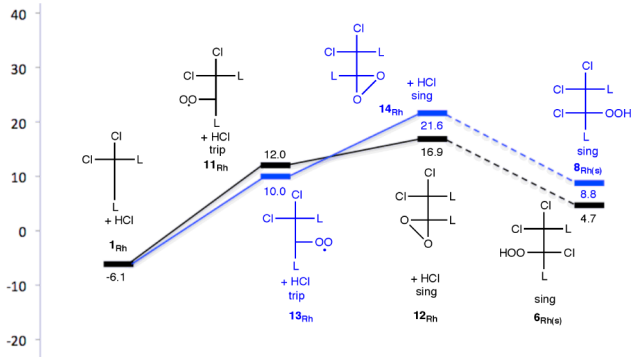

Figure 7. Calculated potential energy surface for the addition of O_2 to the Rh complex, $\mathbf{1}_{Rh}$.

A similar potential energy surface was found for addition of oxygen to $\mathbf{11}_{Ir}$ (Figure 8). The main difference in the Rh and Ir

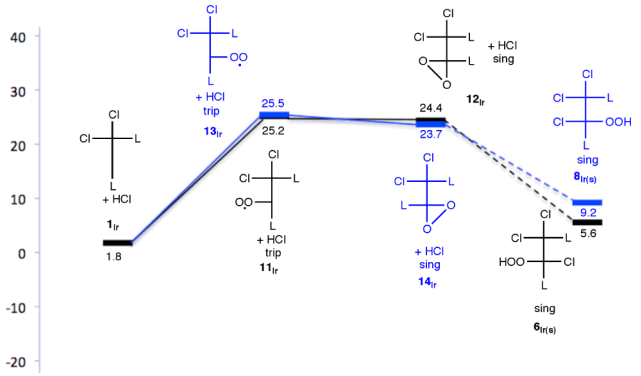

Figure 8. Calculated potential energy surface for the addition of O_2 to the Ir complex, $\mathbf{1}_{Ir}$.

surfaces for oxygen addition is that for the Rh complex the super-oxo is calculated to be more stable than the η^2-peroxo intermediate, while the η^2-peroxo is expected to be more stable for Ir. This is consistent with experimental results for the Ir system as the η^2-peroxo $\mathbf{14}_{Ir}$ was isolated.[21]

Spin Crossover. In an attempt to gain further insight into the triplet/singlet spin-crossing event in the **RE** process, the singlet and triplet surfaces were examined in further detail in the vicinity of $\mathbf{11}_M/\mathbf{12}_M$ and $\mathbf{13}_M/\mathbf{14}_M$ (Figure 9, Table 2). Single-point calculations were performed for species $\mathbf{11}_{Rh(t)}$ and $\mathbf{12}_{Rh(s)}$ with the other spin state and are presented in Figure 9 in order to provide a clear picture of these potential energy surfaces in this region. The corresponding values for all four species in Figure 9 for both Rh and Ir isomers are presented in Table 2.

O_2 Insertion Pathway. Experimental results suggest that the isocyanide ligand, L, is not labile in these systems, although experiments that would directly rule out the loss of L, particularly in the context of O_2 reduction, were inconclusive.[21] One important result mentioned in the experimental paper is that added isocyanide induces decomposition of the starting materials. This prevents the direct testing for inhibition kinetics, which would occur if isocyanide was dissociating prior to RDS. In addition, all NMR evidence suggests strong binding of the isocyanides—for example, any of the asymmetric complexes (such as **1**, **2**, **3**, **6**, and **8**) have two distinct, sharp signals in the ^{1}H NMR spectrum for the two isocyanides.

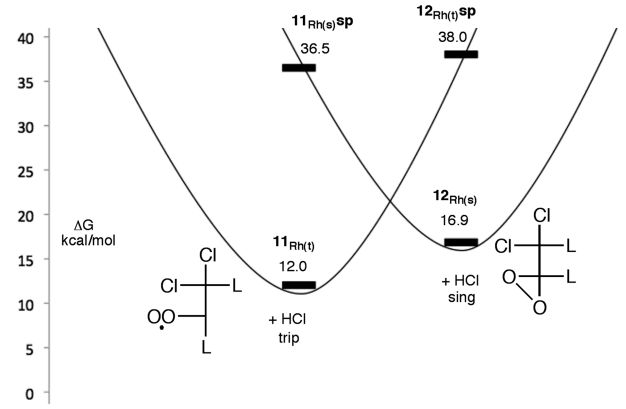

Figure 9. Detailed view of the singlet and triplet surfaces in the vicinity of $\mathbf{11}_{Rh}$ and $\mathbf{12}_{Rh}$. Structures labeled **sp** are single-point calculations performed at the geometry optimized for the other spin state.

Table 2. Energy Values (kcal/mol) for Singlet and Triplet Surfaces in the Vicinity of the Spin crossing for $\mathbf{11}_M/\mathbf{12}_M$ and $\mathbf{13}_M/\mathbf{14}_M$

$\mathbf{11}_{Rh(t)}$	$\mathbf{11}_{Rh(s)}$**sp**	$\mathbf{12}_{Rh(s)}$	$\mathbf{12}_{Rh(t)}$**sp**
12.0	36.5	16.9	38.0
$\mathbf{13}_{Rh(t)}$	$\mathbf{13}_{Rh(s)}$**sp**	$\mathbf{14}_{Rh(s)}$	$\mathbf{14}_{Rh(t)}$**sp**
10.0	35.2	21.6	35.5
$\mathbf{11}_{Ir(t)}$	$\mathbf{11}_{Ir(s)}$**sp**	$\mathbf{12}_{Ir(s)}$	$\mathbf{12}_{Ir(t)}$**sp**
26.6	48.9	25.8	58.9
$\mathbf{13}_{Ir(t)}$	$\mathbf{13}_{Ir(s)}$**sp**	$\mathbf{14}_{Ir(s)}$	$\mathbf{14}_{Ir(t)}$**sp**
26.8	47.5	25.1	60.2

Despite these compelling experimental findings, the $\mathbf{O_2I}$ pathway was still examined computationally. The intermediates formed from the loss of L from $\mathbf{2}_{Rh}$, $\mathbf{15}_{Rh}$, as well as the corresponding O_2 and hydroperoxo complexes, $\mathbf{16}_{Rh}$ and $\mathbf{17}_{Rh}$ (both the singlet and triplet states), were calculated, and their energies are presented in Figure 10. The energies for the corresponding Ir intermediates ($\mathbf{15}_{Ir}$–$\mathbf{17}_{Ir}$) and the intermediates arising from the loss of L from $\mathbf{3}_M$ ($\mathbf{18}_M$–$\mathbf{20}_M$) are presented in Table 3.

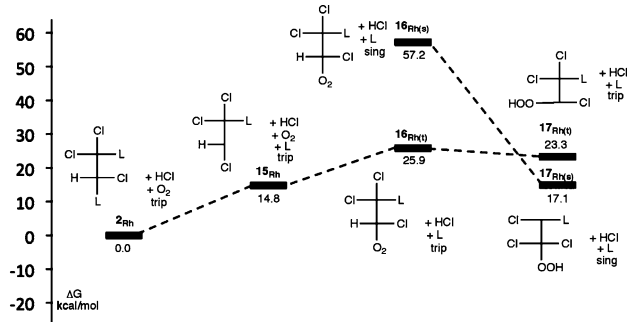

Figure 10. Calculated potential energy surface for O_2I pathway starting from $\mathbf{2}_{Rh}$.

While an examination of the intermediate energies along the singlet and triplet pathways alone is enough to rule out the $\mathbf{O_2I}$ pathway for Ir (Table 3), it is not obvious that this pathway is not accessible on the Rh triplet surface from the intermediates alone. In order to rule out the possibility, the $\mathbf{O_2I}$ transition state was sought proceeding from $\mathbf{16}_{Rh(t)}$. Interestingly,

dx.doi.org/10.1021/ic301303n | Inorg. Chem. 2012, 51, 9499–9507

Table 3. Energy Values (kcal/mol) for Rh and Ir Singlet and Triplet Intermediates along the O_2I Pathway

$\mathbf{2}_{Rh}$	$\mathbf{15}_{Rh}$	$\mathbf{16}_{Rh(t)/(s)}$	$\mathbf{17}_{Rh(t)/(s)}$
0.0	14.8	25.9/57.2	23.3/14.9
$\mathbf{3}_{Rh}$	$\mathbf{18}_{Rh}$	$\mathbf{19}_{Rh(t)/(s)}$	$\mathbf{20}_{Rh(t)/(s)}$
3.9	12.6	19.3/60.8	30.2/17.1
$\mathbf{2}_{Ir}$	$\mathbf{15}_{Ir}$	$\mathbf{16}_{Ir(t)/(s)}$	$\mathbf{17}_{Ir(t)/(s)}$
−1.4	21.9	34.4/56.8	42.0/39.2
$\mathbf{3}_{Ir}$	$\mathbf{18}_{Ir}$	$\mathbf{19}_{Ir(t)/(s)}$	$\mathbf{20}_{Ir(t)/(s)}$
0.0	20.7	33.6/61.0	43.9/32.3

standard transition state searches[25] resulted in a loss of O_2 from the complex and converged to the **HAA** transition state with a vacant coordination site from the loss of L. These results were confirmed with a relaxed scan of the O(β)−H distance starting from $\mathbf{16}_{Rh(t)}$ geometry, which also resulted in the loss of Rh−O_2 coordination and had a maximum consistent with the **HAA** transition state. The energy for this optimized transition state, $\Delta G^{\ddagger}$ = 44.3 kcal/mol, is sufficiently high to rule out this pathway.

A Comprehensive Model: RE vs HAA. When the approximate barriers for reductive-elimination from Figure 4 are combined with the barriers for oxygen addition (Figure 7), a complex picture for the overall **RE** pathway emerges. The Rh isomer $\mathbf{2}_{Rh}$ is found to have two iso-energetic pathways for **HAA** and **RE** (black pathways in Figures 1 and 3) with $\Delta G^{\ddagger}$ = 28.7 kcal/mol. The **HAA** pathway would result in a rate that is first order with complex and first order with oxygen, while the **RE** pathway would be first order in complex only consistent with the second and third terms in eq 1. The other hydride isomer, $\mathbf{3}_{Rh}$, would have a similar barrier of 28.6 kcal/mol for **HAA**, but for the **RE** pathway the initial reductive-elimination step is now lower in energy, resulting in a reductive elimination pre-equilibrium followed by the rate-limiting addition of oxygen, which is consistent with a rate law that is first order in oxygen and complex and inverse first order in HCl, as in the first term from eq 1.

With Ir, however, only one hydride isomer is observed, $\mathbf{3}_{Ir}$. Starting from there, the **HAA** path (blue path Figure 2) has a $\Delta G^{\ddagger}$ = 33.0 kcal/mol compared to the **RE** (blue path Figure 5) with $\Delta G^{\ddagger}$ = 21.5 kcal/mol. This difference of 11.5 kcal/mol would result in a rate law with a **RE** term and no **HAA** term. In addition, oxygen addition is rate-limiting for this RE pathway, resulting in a rate law that is first order in oxygen and complex and inverse first order in HCl, as observed experimentally. Therefore, the determination of whether the **HAA** and **RE** are competitive for both Rh and Ir in these systems seems to originate from the isomer that was employed for the reaction as the energy of $\mathbf{10}_{M}$ is substantially lower in energy than $\mathbf{9}_{M}$ for both Rh and Ir. This factor also determines the rate-limiting step for the **RE** path. These calculations suggest that if the kinetics of the reaction of $\mathbf{2}_{Ir}$ with oxygen were studied, the rate for **RE** would be slowed down and the **HAA** pathway may be found to be competitive.

The theoretical model suggests that the interconversion of $\mathbf{2}_{Rh}$ and $\mathbf{3}_{Rh}$ is accomplished through a **RE**/**OA** pathway proceeding through species $\mathbf{1}_{Rh}$ (eq 3). The barrier for this

$$\mathbf{2}_{Rh} \rightleftharpoons \mathbf{1}_{Rh} + HCl \rightleftharpoons \mathbf{3}_{Rh} \quad (3)$$

interconversion is thus equivalent to the **RE** barrier of Figure 5. The theoretical model further implies that species $\mathbf{2}_{Rh}$ and $\mathbf{3}_{Rh}$ react independently upon the addition of O_2, with species $\mathbf{2}_{Rh}$ responsible for two of the terms in the rate law ($k_1'[\mathbf{2}_{Rh}][O_2]+k_1''[\mathbf{2}_{Rh}]$), while the reaction of species $\mathbf{3}_{Rh}$ produces the term ($k[\mathbf{3}_{Rh}][O_2]/[HCl]$), analogous to what is observed for $\mathbf{3}_{Ir}$. However, the experimental results suggest that the interconversion of $\mathbf{2}_{Rh}$ and $\mathbf{3}_{Rh}$ occurs sufficiently rapidly to give the rate law of eq 1, which only depends on $[\mathbf{2}_{Rh}]$. Considering that the experimental kinetics were (by necessity) conducted in the presence of a large excess of HCl, and that the predicted **RE** pathway for $\mathbf{3}_{Rh}$ includes an inverse first-order HCl dependence, it seems reasonable to suggest that the oxidation of $\mathbf{3}_{Rh}$ occurs at a slow enough rate to allow the isomerization rate to compete, even though the computed standard state reaction barrier for $\mathbf{3}_{Rh}$ is considerably smaller than the barrier for isomerization. If the interconversion of $\mathbf{2}_{Rh}$ and $\mathbf{3}_{Rh}$ was unable to keep pace with the oxidation of $\mathbf{3}_{Rh}$, the experimental kinetics would indicate a biexponential formation of the product, contrary to what was observed experimentally. Thus, it seems that concentration effects, namely the inverse first-order HCl dependence for one of the terms, play a significant role in allowing both hydride isomers to participate in the oxygen reduction reaction and give rise to three parallel reaction pathways.

Computational Methodology. All calculations were density functional theory (DFT) performed with the hybrid functional B3LYP[26,27] as implemented by the Gaussian 09 programming package.[28] All triplet species, as well as the open-shell-singlet single-point species of $\mathbf{5}_{M}$ and $\mathbf{7}_{M}$, were calculated with unrestricted DFT. Rh and Ir were modeled with the effective core potential (ECP) and basis set of Hay and Wadt (LANL2DZ).[29] This ECP basis set was further augmented with the addition of f-polarization functions (exponents = 1.350 and 0.938 for Rh and Ir).[30] All other atoms were modeled using a Pople style[31] double-ζ 6-31G(d′,p′) basis set with polarization functions optimized for heavy atoms.[32]

In addition to this ECP and basis set combination, a small subset of the Rh and Ir reaction profiles was examined with the Stuttgart ECP and basis set,[33] namely species $\mathbf{2}_{M}$ and $\mathbf{TS25}_{M}$ for both Rh and Ir. The ΔE's for these reactions with the original ECP are 17.27 (Rh) and 24.86 kacl/mol (Ir). With the geometries fully optimized with the Stuttgart ECP, the numbers change to 17.35 (Rh) and 23.59 kacl/mol (Ir), differences (0.08 and 1.27 kacl/mol) that are well within the accuracy of DFT. These differences involve a step in which a M−H bond is being broken and where changes to the ECP would likely be the most significant. We therefore conclude that no significant gain would be observed from changing the ECP on the metals.

Slight modifications were made by substituting F for OCH_2CF_3 and $CNCH_3$ for $CNC(CH_3)_3$. Control calculations were performed on species $\mathbf{1}_{M}$, $\mathbf{2}_{M}$,and $\mathbf{3}_{M}$ (M = Rh, Ir), and no substantial changes in the energy or the geometry were observed.

All geometries were evaluated for the correct number of imaginary frequencies through calculation of the vibrational frequencies. From the analytical Hessian, zero point energies as well as enthalpy and entropy corrections for 298.15 K were also calculated and added to the total energy to obtain a total free energy, $\Delta G_{(gas)}[298.15]$.

Intrinsic Reaction Coordinate (IRC) calculations were performed to verify that the optimized transition states do correspond to the proposed intermediates.

Implicit solvent effects were calculated using the polarizable continuum model (PCM)[34] with radii and nonelectrostatic terms from Truhlar and co-workers' SMD solvation model for

dx.doi.org/10.1021/ic301303n | Inorg. Chem. 2012, 51, 9499−9507

geometries optimized in the gas phase.[35] The parameter ε = 7.4257 was used for THF.

Standard state corrections were added to all species to convert concentrations from 1 atm to 1 M. This was accomplished via the equation $\Delta G^{\circ\prime} = \Delta G^{\circ} + RT \times \ln(Q^{\circ\prime}/Q^{\circ})$, where the initial concentration Q° = 1 atm (1/24.5 M for an ideal gas) and the final concentration $Q^{\circ\prime}$ = 1 M.[36] Thus, a value of −1.89 kcal/mol was added to the total free energy for each species. The overall effect of this correction is the addition of $(M - N)$1.89 kcal/mol for the conversion of M molecules to N molecules. This approximation is added in order to better model the changes in solvent phase translational entropy when there are changes in the number of molecules present.

CONCLUSIONS

We performed a detailed density functional study of the reaction of a dirhodium and a diiridium hydride with oxygen with an interest in examining the pathways for oxygen insertion into the metal hydride to form hydroperoxo species. We found that for both the Rh and Ir, an O_2 hydrogen atom abstraction mechanism was possible, but the barrier for the Ir systems was higher by ∼4.5 kcal/mol. This is the first time this mechanism has been applied to Rh and only the second time to any transition metal system other than Pd. While this mechanism was independent of the stereoisomer examined, we found that the competing *trans* HCl reductive elimination pathway was greatly dependent on the stereoisomer examined primarily due to the intermediate formed upon the loss of Cl^-. As a result, the reductive elimination pathway was more favorable for the Ir stereoisomer studied by 11.5 kcal/mol while the two pathways were isoenergetic for the other stereoisomer of the Rh complex. These computational results in total are consistent with the kinetics study previously reported by us (T.S.T. and D.G.N.).[21] We feel that this is a substantial step forward in understanding the factors that govern when this **HAA** mechanism is accessible, which is valuable with respect to catalyst design. In palladium systems, for instance, reductive elimination to Pd^0 can be a pathway to palladium black and catalyst death. In other systems avoiding a coordinatively unsaturated intermediate could be of potential value. An examination of the conversion of these hydroperoxo intermediates to water and oxygen is ongoing.

ASSOCIATED CONTENT

Supporting Information

E, H, and G data for all species and optimized geometries (both Cartesian coordinates and snapshots) for all species have been provided as well as the full reference 25. This material is available free of charge via the Internet at http://pubs.acs.org.

AUTHOR INFORMATION

Corresponding Author

*E-mail: jkeith@lanl.gov.

Notes

The authors declare no competing financial interest.

ACKNOWLEDGMENTS

J.M.K. acknowledges Los Alamos National Laboratory Director's Postdoctoral Fellowship. The Los Alamos National Laboratory is operated by Los Alamos National Security, LLC for the National Nuclear Security Administration of the U.S. Department of Energy under contract no. DE-AC5206NA25396. T.S.T. acknowledges the Fannie and John Hertz Foundation for a graduate research fellowship. D.G.N. acknowledges funding from the NSF (CHE-1112154). J.M.K. would like to thank Nicholas E. Travia for helpful discussion.

REFERENCES

(1) (a) Winter, M.; Brodd, R. *J. Chem. Rev.* **2004**, *104*, 4245. (b) Adler, S. B. *Chem. Rev.* **2004**, *104*, 4791.

(2) (a) Chang, C. K.; Liu, H. Y.; Abdalmuhdi, I. *J. Am. Chem. Soc.* **1984**, *106*, 2725. (b) Collman, J. P.; Wagenknecht, P. S.; Hutchison, J. E. *Angew. Chem., Int. Ed.* **1994**, *33*, 1537. (c) Anson, F. C.; Shi, C.; Steiger, B. *Acc. Chem. Res.* **1997**, *30*, 437. (d) Chang, C. J.; Deng, Y.; Shi, C.; Chang, C. K.; Anson, F. C.; Nocera, D. G. *Chem. Commun.* **2000**, 1355. (e) Chang, C. J.; Loh, Z.-H.; Shi, C.; Anson, F. C.; Nocera, D. G. *J. Am. Chem. Soc.* **2004**, *126*, 10013. (f) Rosenthal, J.; Nocera, D. G. *Acc. Chem. Res.* **2007**, *40*, 543. (g) Soo, H. S.; Komor, A. C.; Iavarone, A. T.; Chang, C. J. *Inorg. Chem.* **2009**, *48*, 10024. (h) Fukuzumi, S.; Kotani, H.; Lucas, H. R.; Doi, K.; Suenobu, T.; Peterson, R. L.; Karlin, K. D. *J. Am. Chem. Soc.* **2010**, *132*, 6874. (i) McGuire, R., Jr.; Dogutan, D. K.; Teets, T. S.; Suntivich, J.; Shao-Horn, Y.; Nocera, D. G. *Chem. Sci.* **2010**, *1*, 411. (j) Dogutan, D. K.; Stoian, S. A.; McGuire, R., Jr.; Schwalbe, M.; Teets, T. S.; Nocera, D. G. *J. Am. Chem. Soc.* **2011**, *133*, 131.

(3) Kaila, V. R. I.; Verkhovsky, M. I.; Wikström, M. *Chem. Rev.* **2010**, *110*, 7062.

(4) (a) Sheldon, R. A.; Arends, I. W. C. E.; ten Brink, G.-J.; Dijksman, A. *Acc. Chem. Res.* **2002**, *35*, 774. (b) Stahl, S. S. *Angew. Chem., Int. Ed.* **2004**, *43*, 3400. (c) Stahl, S. *Science* **2005**, *309*, 1824. (d) Sigman, M. S.; Jensen, D. R. *Acc. Chem. Res.* **2006**, *39*, 221. (e) Gligorich, K. M.; Sigman, M. S. *Chem. Commun.* **2009**, 3854.

(5) (a) Bayston, J. H.; Winfield, M. E. *J. Catal.* **1964**, *3*, 123. (b) Konnick, M. M.; Gandhi, B. A.; Guzei, I. A.; Stahl, S. S. *Angew. Chem., Int. Ed.* **2006**, *45*, 2904. (c) Schlangen, M.; Schwarz, H. *Helv. Chim. Acta* **2008**, *91*, 379.

(6) (a) Konnick, M. M.; Stahl, S. S. *J. Am. Chem. Soc.* **2008**, *130*, 5753. (b) Popp, B. V.; Stahl, S. S. *Chem.—Eur. J.* **2009**, *15*, 2915.

(7) (a) Stahl, S. S.; Thorman, J. L.; Nelson, R. C.; Kozee, M. A. *J. Am. Chem. Soc.* **2001**, *123*, 7188. (b) Konnick, M. M.; Guzei, I. A.; Stahl, S. S. *J. Am. Chem. Soc.* **2004**, *126*, 10212. (c) Landis, C. R.; Moarales, C. M.; Stahl, S. S. *J. Am. Chem. Soc.* **2004**, *126*, 16302. (d) Popp, B. V.; Wendlandt, J. E.; Landis, C. R.; Stahl, S. S. *J. Am. Chem. Soc.* **2007**, *46*, 601. (e) Popp, B. V.; Morales, C. M.; Landis, C. R.; Stahl, S. S. *Inorg. Chem.* **2010**, *49*, 8200.

(8) Szajna-Fuller, E.; Bakac, A. *Inorg. Chem.* **2010**, *49*, 781.

(9) (a) Keith, J. M.; Nielsen, R. J.; Oxgaard, J.; Goddard, W. A., III. *J. Am. Chem. Soc.* **2005**, *127*, 13172. (b) Keith, J. M.; Muller, R. P.; Kemp, R. A.; Goldberg, K. I.; Goddard, W. A., III; Oxgaard, J. *Inorg. Chem.* **2006**, *45*, 9631. (c) Keith, J. M.; Goddard, W. A., III; Oxgaard, J. *J. Am. Chem. Soc.* **2007**, *129*, 10361. (d) Keith, J. M.; Goddard, W. A., III. *J. Am. Chem. Soc.* **2009**, *131*, 1416. (e) Keith, J. M.; Goddard, W. A., III. *Organometallics* **2012**, *31*, 545.

(10) (a) Bakac, A. *J. Am. Chem. Soc.* **1997**, *119*, 1076. (b) Bakac, A. *J. Photochem. Photobiol. A* **2000**, *132*, 87.

(11) (a) Wick, D. D.; Goldberg, K. I. *J. Am. Chem. Soc.* **1999**, *121*, 11900. (b) Look, J. L.; Wick, D. D.; Mayer, J. M.; Goldberg, K. I. *Inorg. Chem.* **2009**, *48*, 1356.

(12) Decharin, N.; Popp, B. V.; Stahl, S. S. *J. Am. Chem. Soc.* **2011**, *133*, 13268.

(13) Denney, M. C.; Smythe, N. A.; Cetto, K. L.; Kemp, R. A.; Goldberg, K. I. *J. Am. Chem. Soc.* **2006**, *128*, 2508.

(14) (a) Popp, B. V.; Stahl, S. S. *J. Am. Chem. Soc.* **2007**, *129*, 4410. (b) Konnick, M. M.; Decharin, N.; Popp, B. V.; Stahl, S. S. *Chem. Sci.* **2011**, *2*, 326.

(15) (a) Chowdhury, S.; Rivalta, I.; Russo, N.; Sicilia, E. *Chem. Phys. Let.* **2007**, *443*, 183. (b) Chowdhury, S.; Rivalta, I.; Russo, N.; Sicilia, E. *Chem. Phys. Lett.* **2008**, *456*, 41. (c) Chowdhury, S.; Rivalta, I.; Russo, N.; Sicilia, E. *J. Chem. Theory Comput.* **2008**, *4*, 1283.

(16) Sha, Y.; Yu, T. H.; Merinov, B. V.; Shirvanian, P.; Goddard, W. A., III. *J. Phys. Chem. Lett.* **2011**, *2*, 572.

(17) Cui, W.; Wayland, B. B. *J. Am. Chem. Soc.* **2006**, *128*, 10350.
(18) Arita, S.; Koike, T.; Kayaki, Y.; Ikariya, T. *Angew. Chem., Int. Ed.* **2008**, *47*, 2447.
(19) Chowdhury, S.; Himo, F.; Russo, N.; Sicilia, E. *J. Am. Chem. Soc.* **2010**, *132*, 4178.
(20) Teets, T. S.; Cook, T. R.; McCarthy, B. D.; Nocera, D. G. *J. Am. Chem. Soc.* **2011**, *133*, 8114.
(21) Teets, T. S.; Nocera, D. G. *J. Am. Chem. Soc.* **2011**, *133*, 17796.
(22) Simões, J. A. M.; Beauchamp, J. L. *Chem. Rev.* **1990**, *90*, 629.
(23) (a) Bakac, A *Inorg. Chem.* **1998**, *37*, 3548. (b) Pestovsky, O.; Veysey, S. W.; Bakac, A *Chem.—Eur. J.* **2011**, *17*, 4518.
(24) Keith, J. M.; Meyerstein, D.; Hall, M. B. *Eur. J. Inorg. Chem.* **2011**, *31*, 4901.
(25) QST2 and QST3 in Gaussian.
(26) Becke, A. D. *J. Chem. Phys.* **1993**, *98*, 5648.
(27) Lee, C.; Yang, W.; Parr, R. G. *Phys. Rev. B* **1988**, *37*, 785.
(28) Frisch, M. J. et al. *Gaussian 09*, revision B.01; Gaussian, Inc.: Wallingford, CT, 2009.
(29) Hay, P. J.; Wadt, W. R. *J. Chem. Phys.* **1985**, *82*, 299.
(30) Ehlers, A. W.; Böhme, M.; Dapprich, S.; Gobbi, A.; Höllwarth, A.; Jonas, V.; Köhler, K. F.; Stegmann, R.; Veldkamp, A.; Frenking, G. *Chem. Phys. Lett.* **1993**, *208*, 111.
(31) (a) Hariharan, P. C.; Pople, J. A. *Chem. Phys. Lett.* **1972**, *16*, 217. (b) Francl, M. M.; Pietro, W. J.; Hehre, W. J.; Binkley, J. S.; Gordon, M. S.; DeFrees, D. J.; Pople, J. A. *J. Chem. Phys.* **1982**, *77*, 3654.
(32) Krishnan, R.; Binkley, J. S.; Seeger, R.; Pople, J. A. *J. Chem. Phys.* **1980**, *72*, 650.
(33) (a) Fuentealba, P.; Preuss, H.; Stoll, H.; Von Szentpaly, L. A. *Chem. Phys. Lett.* **1982**, *89*, 418. (b) Küchle, W.; Dolg, M.; Stoll, H.; Preuss, H. *Mol. Phys.* **1991**, *74*, 1245. (c) Küchle, W.; Dolg, M.; Stoll, H.; Preuss, H. *J. Chem. Phys.* **1994**, *100*, 7535.
(34) Tomasi, J.; Mennucci, B.; Cammi, R. *Chem. Rev.* **2005**, *105*, 2999.
(35) Marenich, A. V.; Cramer, C. J.; Truhlar, D. G. *J. Phys. Chem. B* **2009**, *113*, 6378.
(36) Cramer, C. J. *Essentials of Computational Chemistry*, 2nd ed.; Wiley: Chichester, U.K., 2004; p 378.